Sensible heat flux and boundary layer depth measurements by Doppler SODAR and sonic anemometer data (*)

G. CINQUE (1)(2), R. ZAURI (2), P. DI CARLO (2)
M. IARLORI (2) and V. RIZI (2)

(1) *Istituto Nazionale di Geofisica - L'Aquila, Italy*
(2) *Dipartimento di Fisica, Università di L'Aquila - L'Aquila, Italy*

(ricevuto l'1 Febbraio 1999; revisionato il 16 Febbraio 2000; approvato il 21 Marzo 2000)

Summary. — A validation of a simple mixed-layer similarity relationship, firstly proposed by Panofsky and McCormick (1960), is presented for wind speeds up to $7\,\mathrm{ms}^{-1}$ and over an uneven terrain. The surface heat flux and the Planetary Boundary Layer depth, z_i, are retrieved from this relationship, by using SODAR measurements of the vertical velocity variance σ_w^2, under the hypothesis that the heat flux linearly decreases with height. All the measurements are relative to days characterized by high-pressure conditions, during periods of well-developed convection. The values of the surface heat flux obtained from such a method are compared with those obtained by applying the eddy correlation technique to the vertical wind velocities and virtual temperatures measured by a sonic anemometer. The values of z_i obtained from the same relationship are compared with the height of the lowest inversion layer estimated from the facsimile record of the echoes received by the vertical antenna of the SODAR. The spectral behavior of vertical and longitudinal wind velocity from the anemometer and the SODAR is examined, too. In such a way an independent estimate of z_i is obtained from the position of the spectral maximum.

PACS 92.60 – Meteorology.
PACS 92.60.Fm – Boundary layer structure and processes.
PACS 92.60.Ek – Convection, turbulence and diffusion.

1. – Introduction

In the last few years, due to the decreasing costs and increasing performances of remote-sensing instruments able to measure the wind vector and the temperature in the first kilometer of the atmosphere, there has been a new interest in the study of this portion of the troposphere, that is usually called Planetary Boundary Layer (PBL). This name derives from the fact that the earth's surface is a boundary on the domain of the atmosphere and that the atmospheric layers close to this boundary behave in a quite different manner than the rest of the troposphere.

(*) The authors of this paper have agreed to not receive the proofs for correction.

There are various ways to define the PBL. One of the most used is that given by Stull [1]: "The PBL is that part of the troposphere that is directly influenced by the presence of the earth's surface, and responds to surface forcing with a time-scale of about an hour or less".

The forcing is due to the combined action of radiative heating or cooling, heat transfer processes and frictional drag or strains induced by terrain complexity.

The principal source of this forcing is, of course, the solar radiation that in a more or less direct way drives all the motions of the atmosphere. However, just a negligible amount of solar radiation is absorbed directly by the atmosphere; most is absorbed by the ground, which via turbulent exchange transport processes supplies the heating/cooling of the PBL. Turbulence is the most important transport process in the PBL, while it is practically absent in the free atmosphere. It is for this reason that the free atmosphere is unable to respond quickly to the surface forcing and that turbulence is also often used to define the PBL itself.

Since the earlier studies of turbulence in the lower atmosphere, the variance of the vertical wind component, σ_w^2, was widely used to obtain information concerning the evolution of PBL. For this purpose several similarity relationships have been proposed and validated, involving, besides σ_w^2, other relevant PBL parameters.

In the present work we investigate on the ability of a simple similarity relationship, firstly proposed by Panofsky and McCormick (1960) [2] to evaluate the Sensible Heat Flux (SHF) profile during periods characterized by convection and low wind speed, *i.e.* when shear production of turbulence can be neglected with respect to buoyancy production.

This relation can be expressed as

$$\frac{\overline{\sigma_w^3}}{z} = \beta \frac{g}{\overline{\theta}_v} \overline{w'\theta'_v}, \tag{1}$$

where $\overline{w'\theta'_v}$ is the turbulent virtual potential temperature flux or SHF in cinematic units, $\overline{\theta}_v$ is the virtual potential temperature, g is the acceleration due to gravity, z is the height above ground and $\beta = 1.66$ is a universal constant [3]. Using this relation, we are able to retrieve the vertical sensible heat flux profile from SODAR measurements of the profile of σ_w^2. The values of SHF at the surface are obtained extrapolating the linear part of this profile down to the ground. A more detailed description of the method is given in subsect. 3·1.

We have already mentioned the importance of Sensible Heat Flux in the coupling between soil and the atmospheric layers in contact with it. In fact, the numerical weather prediction models are able to resolve just the largest scale motions; the smaller scale motions (or turbulence) are not modeled directly, but are parameterized by subgrid-scale approximations. Thus, a correct parameterization of SHF, together with turbulent flux of momentum and moisture, is of fundamental importance in weather and climate numerical forecasting models, for long- , medium-range or severe weather forecasts.

SHF appears in similarity relationships useful to obtain other PBL parameters such as the mixed layer height h and the temperature structure parameter C_{T^2} [4]. An estimation of SHF from SODAR measurements starting from (1) has been performed in the past few years by several authors [3-6]. They show that SHF values obtained from SODAR agree with those obtained with other techniques in the limit of 10–20%. However, their results were relative to near ideal conditions, *i.e.* for flat sites and with

very low wind intensities (1–2 m/s). Even if our experimental conditions are not so strictly ideal, however we can test the reliability of the estimates of the ground SHF values obtained from such a procedure. It can be done thanks to the availability of reference values for the ground SHF obtained with an independent method for the same time periods.

In fact, the values of ground SHF obtained by applying the eddy correlation technique to the vertical wind velocities and temperatures measured by fast response sensors, such as sonic anemometers, constitute probably the better reference that can be used for comparison (due to the necessity of collecting a very large amount of data, this method is rarely used for routine measurements). So it was straightforward decided to validate the similarity relationship by a comparison with SHF values obtained from such a method.

In a previous work [7], we have shown that the diurnal trends of the SHF and of the friction velocity calculated with the eddy correlation technique for the same site agree very well with those obtained from different numerical models of the PBL. The horizontal spatial resolution of the models was of 3 km. This result may justify the reason for the comparison, as the values of SHF measured by the sonic anemometer seem to be representative of the mean values on the local scale.

On the other hand, we have obtained from the same similarity relationship an estimate of the PBL depth z_i. It was done by extrapolating the upper part of the linear profile of the SHF up to the height, z_h, at which it intercepts the z-axis, *i.e.* when the linear SHF becomes zero. It is important to point out that nevertheless z_h constitutes a rough estimate of the Mixed Layer depth, however a simple relation exists that links z_h and z_i [8]:

$$z_h/z_i \approx 0.7\,. \tag{2}$$

The PBL height z_i is defined as the height of the ground-based temperature inversion. It is well known that the contemporary occurrence of temperature inversion and wind shear gives rise to strong values of the backscattered echo intensity, especially as far as the vertical antenna is concerned. Since a relatively strong wind shear is often present in the entrainment zone, *i.e.* the shallow zone through which entrainment processes between the PBL and the free atmosphere occur [9], the PBL height z_i is often visible in the SODAR facsimile plot, as the height corresponding to the lower dark zone [3], [4] and [9].

The matching between the evaluations of z_i obtained by the extrapolation of the SHF profile and inferred from the analysis of the facsimile records depends on a reliable choice of the linear interval used for the best-fit interpolation.

Unfortunately there were only few occasions (in the early morning) for which the inversion height was obtainable from the facsimile record. So we have decided to perform the spectral analysis of the vertical and longitudinal wind velocities obtained by the SODAR for different range gates. The same analysis, for some of the time periods, was performed also on the anemometer data, for a comparison purpose.

The aim of such a procedure was to infer an estimate of the PBL depth, z_i, by using the empirical relationship firstly developed by Kaimal *et al.* [9-11],

$$\lambda_{\mathrm{m}} \approx 1.5 z_i\,, \tag{3}$$

that relates the wavelength of maximum energy, λ_{m}, in the u- and w-spectrum to the boundary layer height z_i. A detailed description of the procedures followed to draw spectra and to estimate λ_{m} will be given in subsect. 3·3.

2. – The site and experimental setup

The field campaign has been performed during various short periods: 16-18 Jan, 6-7 Feb, 22-24 Apr and 13-17 May 1998. Even if all these days were characterized by high-pressure conditions, we have discarded the ones for which a non-negligible presence of clouds and strong acoustic noise in the central hours was observed.

The instruments were installed at Preturo (42.38 N, 13.32 E and 683 m a.s.l.), about 8 km NW of L'Aquila, in the middle of a gently rolling valley surrounded by the mountains of the Appennino Abruzzese. The site is however almost flat in a radius of about 3 km. A map of the site, showing contour levels, is reported in fig. 1. This map is drawn from level data taken with a horizontal resolution of 10 m (the altitude accuracy is of 1 m). The ridge of the Gran Sasso mountain, approximately 20 km N-E of Preturo and not visible in fig. 1, is almost parallel to the valley profile. A vectorial plot, slightly degraded both in time and height resolution, representative of the SODAR measured winds for each of the day under analysis, is shown in fig. 2.

Due to the presence of the small buildings which houses the computers and the indoor instrumentation and to the presence of trees and isolated houses on each side, the site is not free of small scale surface obstructions and of sporadic acoustic noise.

2·1. *The SODAR.* – The SODAR is a model APM-400 ES made by Multimicro (Rome, Italy). It is a triaxial, monostatic, Doppler SODAR, with three electro-acoustic transducers, each emitting an acoustic burst at a different frequency (respectively:

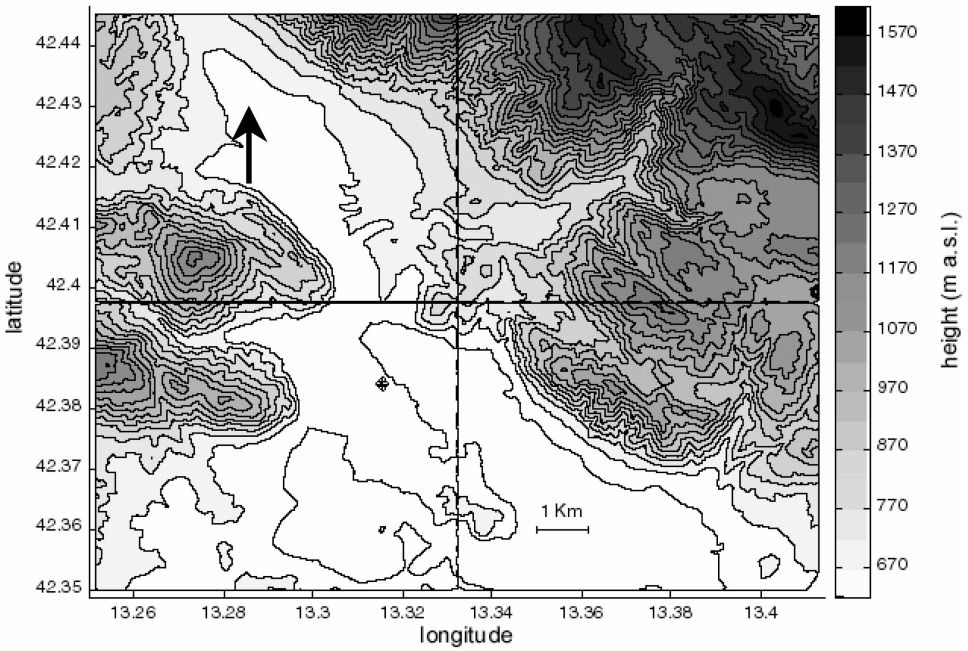

Fig. 1. – Map of the Aterno river valley, showing contour levels with a height resolution of 50 m. The diamond indicates the exact SODAR location, while the peak in the lower right corner is relative to the higher part of L'Aquila.

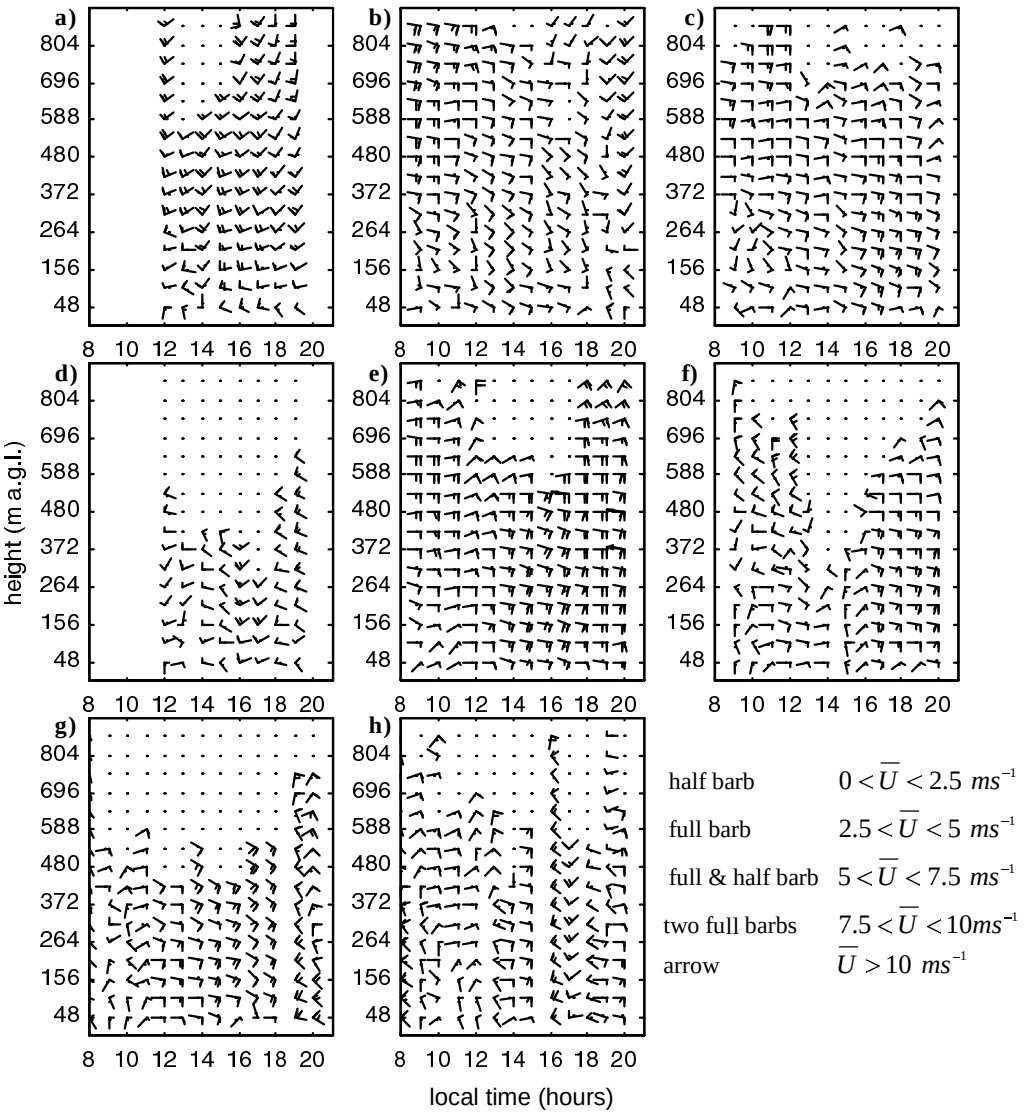

Fig. 2. – Time-height profiles of the mean horizontal wind $\overline{U}$ for a) Jan 16, b) Jan 18, c) Feb 6, d) Feb 27, e) Apr 23, f) May 13, g) May 14, h) May 15, 1998. North direction is upward.

1750, 2000, 2250 Hz). In this way it is possible to carry out the spectral analysis of the three echoes in one step.

The acoustic pulse has a power of 50 W (r.m.s.) and a length of 100 ms. It is fired every 6 seconds. The signals are digitized online at 1600 samples per second. The frequency shift of the echoes is obtained by applying a fast Fourier transform to the digitized return signal, using 256 points for each range gate. For each burst the data have been recorded at 31 levels, each of them having a vertical resolution of 27 m.

Due to the delay in the opening of the receiver gate and the total number of points analyzed, the first interval was at a height of 39 m and the highest at 850 m.

To evaluate the Doppler shift of the echoes frequencies a two-step numerical process on the spectra of the backscattered signals from each range gate is used [12]. The spectral analysis is also used to build up facsimile plots.

The mean wind profile, the standard deviation of the mean wind components as well as parameters for evaluating the data's quality are calculated every 20-30 minutes. The software also gives the criterions for accepting or rejecting the signal and for the spike removal in the moment calculations. These criteria, together with a more detailed description of the acquisition software, are described in [12].

2·2. *The sonic anemometer.* – We used a sonic anemometer made by Gill-Solent Research. The measuring head is composed of three pairs of ultrasonic transducers, and is placed at the top of a 10 meter mast. It is located in Preturo too, at a distance of about 20 m from the SODAR. Each pair of transducers operates alternatively as transmitter and receiver of high-frequency ultrasound pulses. The anemometer shots an ultrasonic pulse every 1 ms. This firing is repeated for the two directions of each sonic axis. The mean value (calculated on eight sets of firings) of the two transit time counts along each axis is sent to a PC for further processing. The software permits to correct and calibrate the three vector speeds, in order to take into account the obstruction effects of the framework and transducers. It also performs the rotations to give the three wind components referred to an orthogonal system. Data of the three wind orthogonal components and the speed of sound are stored on the PC at a sampling rate of 21 Hz.

The main information obtained from the sonic anemometer is the direct calculation of turbulent fluxes of sensible heat and momentum performed using the eddy correlation technique (see subsect. 3·2).

2·3. *Low-frequency measurements.* – A platinum resistance thermometer with a nominal resistance of 100 Ohm (PT100) and a thin film hygrometer are placed on the same mast of the anemometer. The value of the mean temperature from the PT100 and of the mean relative humidity from the hygrometer, calculated over a period of 10 min, were stored on a data logger. These values are the ones used to calculate $\overline{\theta}_v$ in (1).

3. – Analysis techniques

3·1. *The linear regression method.* – We have already seen in the introduction that (1) holds just when the shear production of TKE is negligible if compared to that generated by convection.

However, the starting point to get (1) is the equation of the average TKE. This equation, if we assume a coordinate system aligned with the mean wind, horizontal homogeneity and no subsidence, can be written as

$$\frac{\partial \overline{e}}{\partial t} = \frac{g}{\overline{\theta}_v} \overline{w' \theta_v'} - \overline{u' w'} \frac{\partial \overline{U}}{\partial z} - \frac{\partial(\overline{w' e'})}{\partial z} - \frac{1}{\overline{\varrho}} \frac{\partial(\overline{w' p'})}{\partial z} - \varepsilon \,, \tag{4}$$

where $\overline{e} \equiv (1/2)(\overline{u'^2} + \overline{v'^2} + \overline{w'^2})$ is the mean TKE, $\overline{w' \theta_v'}$ is the turbulent flux of virtual potential temperature, $\overline{u' w'}$ is the turbulent flux of momentum, $\overline{w' e'}$ is the turbulent flux of TKE, θ_v is the virtual potential temperature, $\mathrm{d}\overline{U}/\mathrm{d}z$ the mean wind shear, $\overline{\varrho}$ is

the density of air, u' and w' are the turbulent fluctuations of longitudinal and vertical velocity components about their mean value.

The term on the left-hand side of (4) represents the local change of TKE, while the terms on the right represent buoyant and mechanical production, turbulent transport, pressure perturbations and viscous dissipation, respectively. A more detailed description of each term in (4) can be found in [1] and [5].

Panofsky and McCormick (1960) [2] and Caughey and Readings (1974) [13] have considered that, in convective conditions, the prevailing terms in the TKE budget are the ones relative to buoyant and mechanical production. Under the hypothesis that in the mixed layer the shear production of turbulence is much less than buoyant production and assuming steady state of meteorological conditions, (4) can be written as

$$\frac{g}{\overline{\theta}_v}\,\overline{w'\theta'_v} \approx \varepsilon\,. \tag{5}$$

As in a developed turbulent regime [18]

$$\varepsilon \propto \frac{\sigma_w^3}{z}\,, \tag{6}$$

starting from (5) we obtain (1).

Besides, $\overline{w'\theta'_v}$ decreases linearly with height in the well-mixed layer [1], [4] and [5]. Because of the direct proportionality between σ_w^3/z and $\overline{w'\theta'_v}$, the vertical profile of σ_w^3/z will be linear too, resulting in

$$\frac{\sigma_w^2(z)}{z} = \beta\,\frac{g}{\overline{\theta}_v}\,\overline{w'\theta'_{v_0}}\left(1 - \frac{z}{z_h}\right), \tag{7}$$

where $\overline{w'\theta'_{v_0}}$ is the surface heat flux and z_h is the height at which the heat flux vanishes by linear extrapolation.

Fitting the linear part of the σ_w^3/z profile with a least-square straight line, it is possible to extrapolate it up to intercept the z-axis, to obtain an estimate of z_h [14]. Once z_h is known, z_i can be drawn by (2). In fact, the usual characteristic length in the well-mixed layer similarity is z_i. The z_i values obtained from such a procedure are compared with the few ones obtained from spectral analysis or facsimile plots.

The linear profile of heat flux obtained from eq. (7) can also be extrapolated down to the surface layer. The value of $\overline{w'\theta'_v}$ at 10 m is compared to that determined by the sonic anemometer by using the eddy correlation method.

3·2. *The eddy correlation method.* – We have seen that the principal advantage of the sonic anemometer derives from the simultaneous measurements of velocity and temperature fluctuations, the last ones being derived from the speed of sound. So it is immediate to calculate turbulent fluxes from sonic anemometer's output data via the eddy correlation method, even if some problems arise because of the humidity dependence of the speed of sound.

The eddy correlation method gives a direct estimation of turbulent fluxes. The sensible heat flux is given by [1]

$$H = \overline{\varrho} C_p \overline{w'\theta'} \tag{8}$$

where $\overline{\varrho}$ is the mean density of air, C_P is the specific heat for moist air at constant pressure, w' and θ' are vertical velocity and potential temperature fluctuations around their mean value.

The relation between sonic temperature and true temperature turbulent fluxes, $\overline{w'T'_s}$ and $\overline{w'T'}$, has been studied by many authors [15-17]. Their analysis shows that, for a dry convective PBL, $\overline{w'T'_s}$ constitutes a reasonable estimate of $\overline{w'T'}$. We are however interested just to the virtual potential temperature turbulent flux $\overline{w'\theta'_v}$. As $\theta_s \approx \theta_v$, we have that $\overline{w'\theta'_s} \approx \overline{w'\theta'_v}$.

Before calculating the product $\overline{w'\theta'_s}$ we have performed the standard two-dimensional rotation to align the axis of measure with the streamline. The averaging time was set in 20 or 30 minutes, depending on the averaging time chosen for the contemporary SODAR measurements. The detrending of temperature was performed by simple subtracting the mean values $\overline{\theta_s}$ calculated during the same period ($\overline{w} = 0$ because we are in the streamline system), as is common practice.

3·3. *Spectral analysis.* – Our SODAR can work with two different types of acquisition software. The first one, usually employed for routine measurements, gives as output just the mean value and standard deviations of the vertical component, the horizontal wind speed and direction as well as the percentage of validated data used in the calculation of first- and second-order momentum. The second, together with the mean values, gives also the instantaneous values of the wind components and the respective signal-to-noise ratio relative to each antenna.

The only two days analyzed with the latter software were January 16, 1998 and February 27, 1998. For these days we have performed the spectral analysis of the wind components measured from both SODAR and anemometer. The components of the wind vector were rotated in order to align the u axis with the streamline, for both SODAR and anemometer.

For the spectral analysis of the anemometer data, we have followed a procedure similar to the one used in [10]. The data were first degraded by taking the mean value every 7 points. The total amount of data is thus reduced and a criterion for spikes removal can be applied, with essentially no information losses. In this manner the frequency of acquisition is reduced to 3 Hz. The spectral analysis of each time series is performed for two separate, partially overlapping, frequency subranges. The high-frequencies spectra, ranging from about $3 \cdot 10^{-3}$ Hz to 1.5 Hz, are retrieved by applying an FFT algorithm to 11 consecutive time periods of 1024 points (≈ 6 min). The 11 spectra so obtained are then block averaged to give the final spectrum representative of the whole period (≈ 63 min). To obtain the low-frequencies spectra, ranging from about $3 \cdot 10^{-4}$ Hz to $1.4 \cdot 10^{-1}$ Hz, we have performed an ulterior degradation of the data, by taking the mean value every 11 points. The FFT was then computed on this twice time-degraded series.

Both high- and low-frequency spectra were smoothed. The agreement between the two spectral components in the overlapping region was generally quite good; nevertheless we have tuned the two spectra by imposing the same mean value. The transition point from one spectrum to the other was set at 10^{-2} Hz.

As far as the SODAR data are concerned, a 512-point Fast Fourier Transform (FFT) routine was used to compute spectra for each range gate. The missing data in the time series, due to the rejection of unsatisfactory signal-to-noise ratio, have been interpolated by means of a third-order spline. Since the sampling period was of 6 s, each spectrum is relative to a period of about 52 min. The time series of sonic

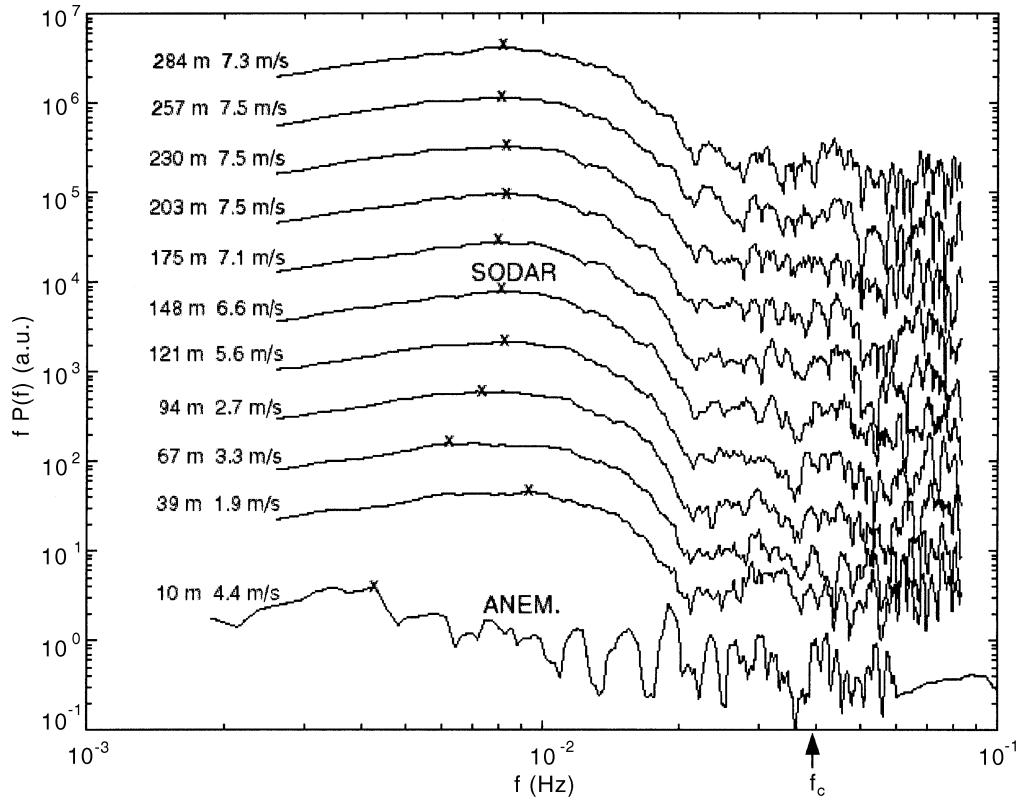

Fig. 3. – u-spectra between 13.39 and 14.31 of January 16, 1998 (the lower one is relative to the anemometer while the SODAR ones are scaled for the sake of clarity). The mean height and velocity relative to each range gate of the SODAR and to the anemometer are shown at the left of the corresponding spectra. The crosses indicate the position of the spectral maxima.

anemometer and SODAR data, having slightly different lengths, start at different times in order to have nearly the same central point. The longitudinal and vertical velocity spectra relative to each range gate of the Sodar and to the sonic anemometer for one of the considered time periods are displayed in fig. 3 and 4, respectively. The u-spectra, according to other authors [8-10], display a shift of the power maximum toward higher frequencies as a function of increasing height in the surface layer or, more precisely, for $0 < z < 0.1 z_i$. Thus, taking into account the $U(z)$ profile, a quite univocal estimate of the boundary layer depth, z_i, should result from the application of eq. (3) to each range gate. However we have found that, as far as the lower heights are concerned, just the spectra relative to the anemometer roughly show the right displacement, as can be observed by looking at fig. 3.

The w spectra, as formerly observed by Greenhut and Mastrantonio [3], exhibit the power maximum at a roughly constant frequency. In fact, (3) holds for w-spectra just in the limit $0.1 z_i < z < z_i$ [9, 10]. Furthermore, for wind speeds ranging from 4 to 8 ms^{-1} over uneven terrain, (3) is adequate for $0.4 z_i < z < z_i$, while in the lower part of the mixed layer the w-spectra are expected to linearly scale with z [10].

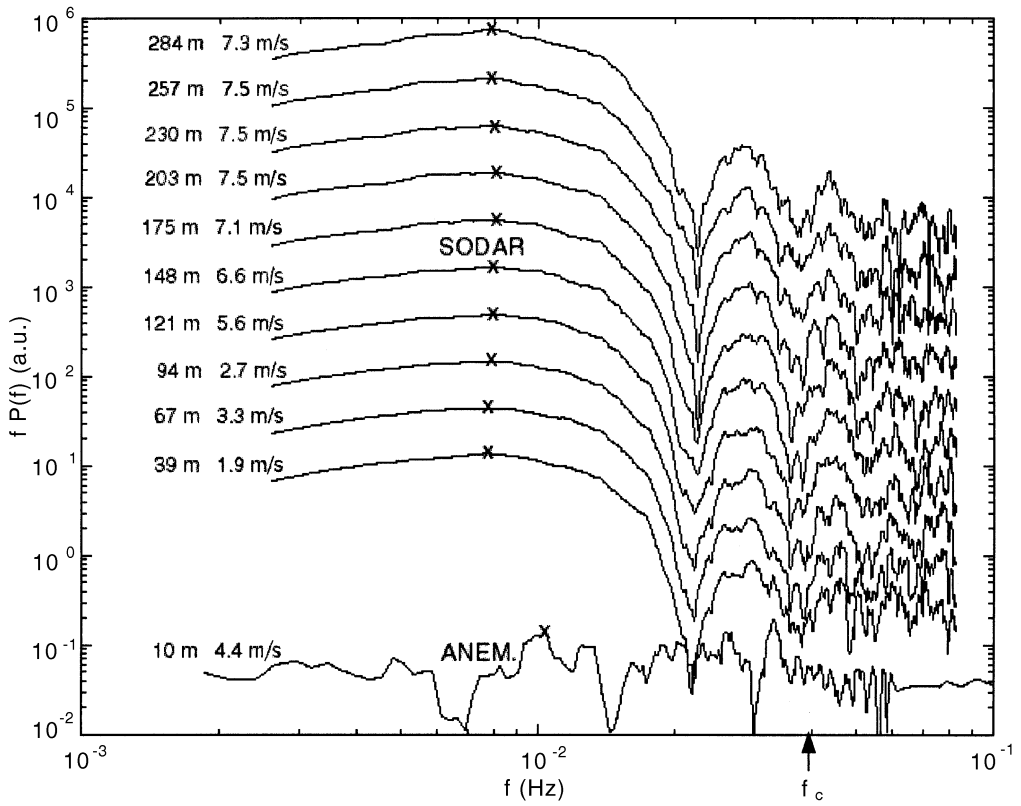

Fig. 4. – As in fig. 3 but for the w component.

In our cases the w-spectra maximum shift with z toward higher frequencies at the lowest SODAR levels was not observed. We have then used (3) for both the u- and w-spectra, but considering just the mixed layer, *i.e.* the height region characterized by an almost constant wind speed.

In the sample case shown in fig. 3 we obtain from the u-spectra $z_i = 585$ m with a standard deviation of 25 m, while from the contemporary w-spectra shown in fig. 4 we obtain $z_i = 580$ m with a standard deviation of 30 m. These values are in good agreement with the facsimile plot that shows, during the same time period, thermals reaching a maximum height of about 550 m.

Unfortunately, for the lower PBL heights we must consider just the spectra relative to the first range gates, thus obtaining standard deviations as large as $z_i/3$. Furthermore, probably due to the high variability with time of the wind direction and intensity at such low levels, the corresponding spectra showed the presence of several wide maxima, also for frequencies lower than 10^{-2} Hz. We have then somewhat arbitrarily computed λ_m as the wavelength corresponding to the maximum of the well-defined peak at the lower-frequencies side of the u-spectra.

Some considerations are necessary as far as SODAR spectra are concerned. We must keep in mind that SODAR measurements are representative of the volume illuminated by the acoustic beam during the time interval of the measure. Even if the

spectra are expressed in terms of frequency, however, by invoking the Taylor hypothesis, the frequency can be related to the characteristic wavelength of eddies (or eddy size) λ. So, the volume averaging has the effect of a low-pass filter. Weill [4] defined a cut-off frequency f_c through the relation

$$f_c = \frac{\overline{U}}{2\pi z \tan\alpha}, \tag{11}$$

where $\overline{U}$ is the mean wind velocity, z is the height and α is the half-beam width of the antenna. Taking into account typical values of the periods analyzed, *i.e.* $\overline{U} = 5\ \mathrm{ms}^{-1}$, $z = 300$ m and $z\tan\alpha = 30$ m, we obtain from (11) $f_c = 2.7 \cdot 10^{-2}$ Hz. Since our spectral maxima are at lower frequencies, it seems reasonable to estimate z_i from such a method.

The u- and w-spectra relative to sonic anemometer data show that the lower limit of the inertial sub-range occurs at frequencies higher than 10^{-1} Hz (fig. 5). Therefore the velocity spectra obtained from the SODAR time series cannot display the inertial sub-range as a consequence of the high-frequency cut-off (at about 0.08 Hz) set by echoes sampling time.

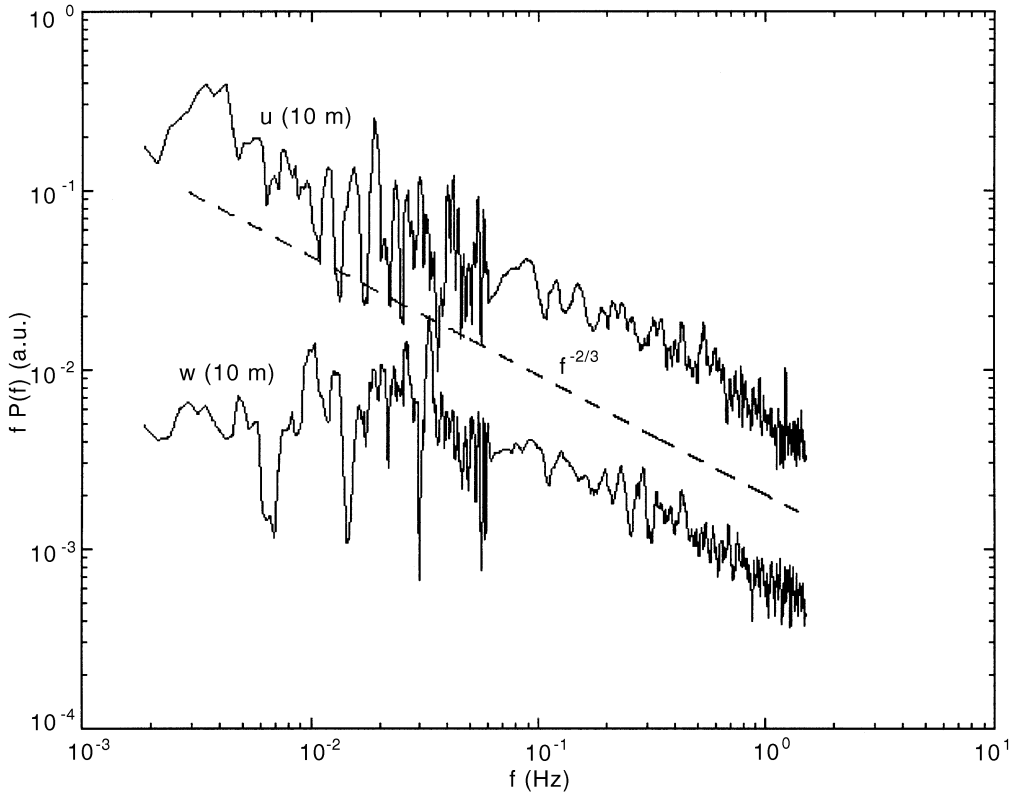

Fig. 5. – u- and w-spectra from the anemoemeter's data between 13:34 and 14:36 of January 16, 1998.

4. – Observations and results

4·1. *Preliminary considerations.* – The days selected for the present analysis were characterized by fair weather and free convection in the central hours of the day, as is clearly visible, for three of the eight analyzed days, in the facsimile plots displayed in fig. 6.

Most cases display a linear behavior of σ_w^3/z in the central part of the mixed layer, that is less sensitive to terrain-induced flow modifications and to the effect of entrainment (fig. 7a, b, d, e). The linear fitting was made, generally, by taking about 7 points (never less than 5, anyway) with an average correlation coefficient of about 0.95.

Sometimes, in spite of claimed convection, σ_w^3/z does not exhibit a linear behavior (fig. 7c). The perturbation of the mixed-layer turbulent structure should be originated by non-stationary meteorological conditions. In the specific case an evident rotation of the wind starts just at 13:30 (fig. 8). This feature is probably due to the rising of a volley-mountain breeze or some other geographically generated effect that strongly interacts with the previous flow. The presence of non-stationary conditions, when it is

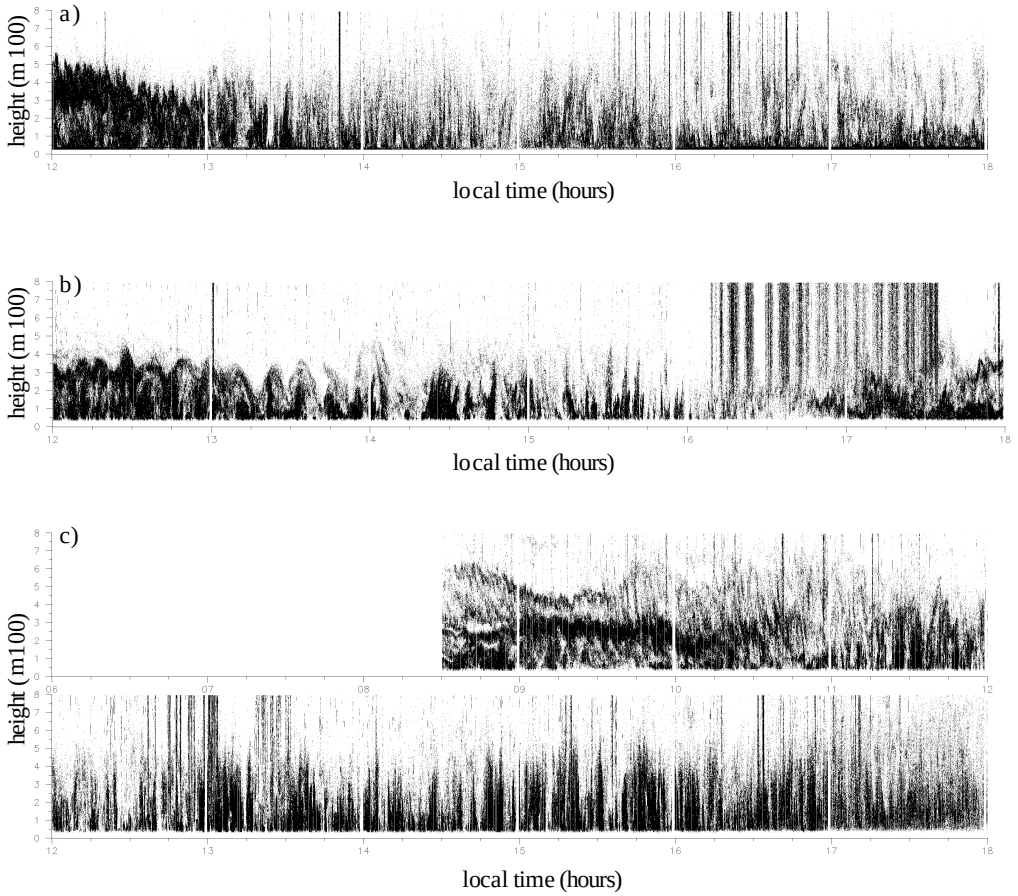

Fig. 6. – Facsimile plots of a) January 16, b) February 27, c) April 23, 1998.

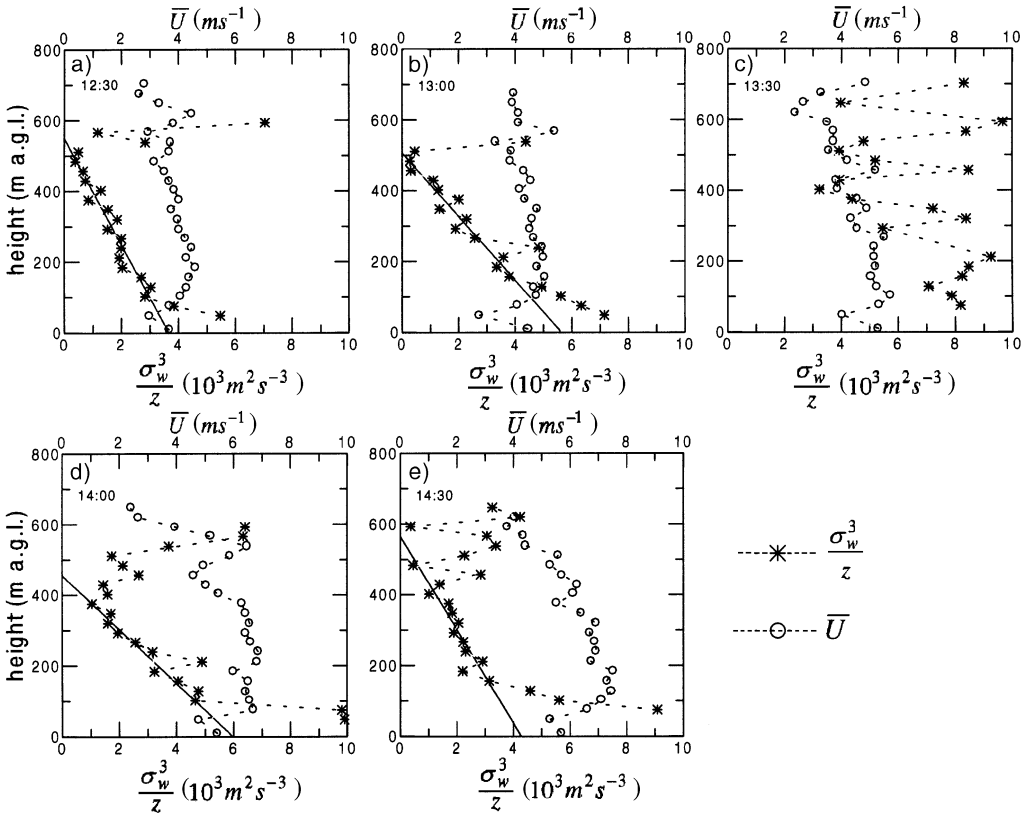

Fig. 7. – σ_w^3/z and mean wind profiles for April 23, 1998.

due to convergence-divergence on a local scale, should be detected from the $\overline{w}$ behavior. A $\overline{w}$ time-height profile at 13:30, showing a pronounced difference in comparison with profiles relative to previous and following time periods, can indeed be observed in fig. 9. Looking at fig. 2, we can also note that a more or less pronounced change of the wind direction and/or intensity occurs, during the central hours, at least once for each day of analysis. It was then an expected feature to find the absence of linearity in the σ_w^3/z profiles relative to these time periods, as quasi-stationarity is a necessary condition for (1) to hold.

There are other causes that can lead to a missing or non-significant linear σ_w^3/z profile. In order to illustrate these causes, we can again consider the sample case of April 23, 1998. Most of the σ_w^3/z profiles displayed in fig. 7 show the presence of a linear trend also for heights lower than the ones chosen for the fit. This feature was common to many of the time periods of the other days. We have at first checked that the choice of the lower linear profile would often, but not always, lead to unreliable values for the extrapolated SHF. Subsequently, to better understand the nature of such a behavior, we have computed the values of the friction velocity u_*, the Monin-Obukov length L and of the turbulent vertical flux of longitudinal momentum $\overline{u'w'}$, by using just anemometer's data. The gradient of the surface wind $\partial\overline{U}/\partial z$ was subsequently obtained by using the Businger-Dyer similarity relationship for unstable conditions $\partial\overline{U}/\partial z =$

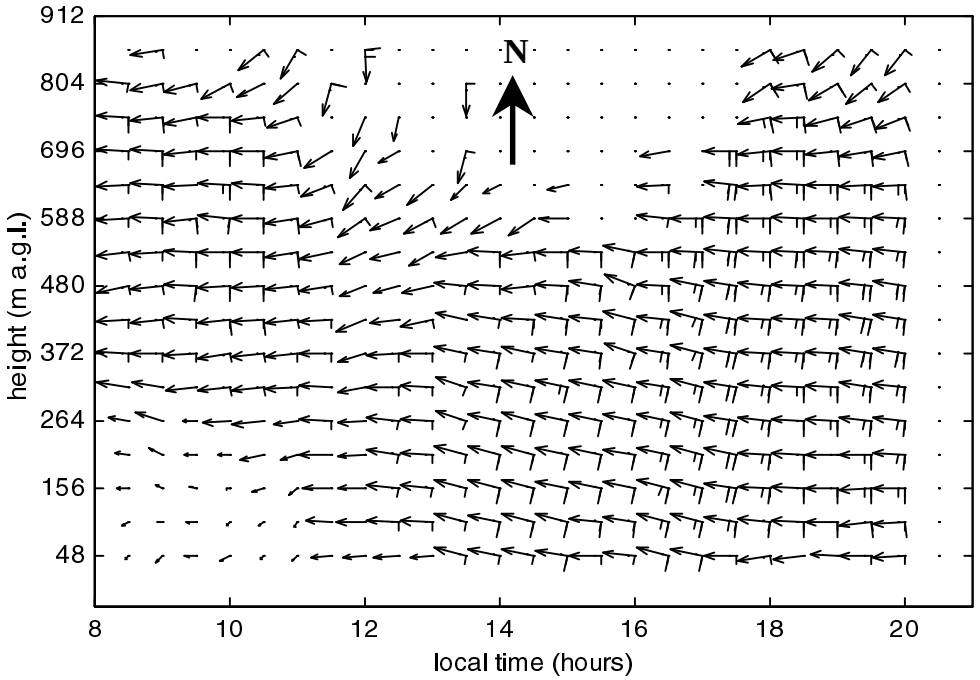

Fig. 8. – Time-height profiles of the mean horizontal wind $\overline{U}$ for April 23, 1998. For $0 < \overline{U} < 4\,\mathrm{ms}^{-1}$ the arrow length is proportional to $\overline{U}$; for $4 < \overline{U} < 12\,\mathrm{ms}^{-1}$ the $\overline{U}$ values are divided into four classes $2\,\mathrm{ms}^{-1}$ wide, where the passage from one class to the successive is denoted by adding a half-barb (two half-barbs correspond to a full barb).

$(u_*/kz)[1 - (15z/L)]^{-1/4}$, where k is the dimensionless von Karman constant [1]. Following [1] we have taken $k = 0.4$.

The relevant results from such an analysis are the following:

i) If $\xi = \dfrac{(g/\overline{\theta}_v)\,\overline{w'\theta'_v}}{\overline{u'w'}(\partial\overline{U}/\partial z)}$ is the ratio between the buoyancy and shear production term of the TKE equation (4), we have found $0.2 < |\xi| < 2$ in most of the cases with a linear σ^3/z profile.

ii) Values of $|\xi| > 5$ often occur in the first morning hours, *i.e.* from about two hours after sunrise to about an hour before the first vigorous thermals become visible in the facsimile plot.

iii) Due to the relatively high values of the friction velocity, we have found $-1 < (z/L) < 0$ in a wide number of time periods characterized by SHF values ranging from 30 to $100\,\mathrm{W\,m}^{-2}$.

Moreover, in the early morning the facsimile plots of fig. 6 show a PBL height of about 150 ± 100 m. Due to the surface shear production and height resolution of the SODAR, we have concluded that the method of profile flux extrapolation was not applicable for such a low PBL height, unless a surface wind lower than $1\,\mathrm{ms}^{-1}$ and a surface-based inversion higher than 200 m were present. In other words, for most of the days under consideration, the early morning hours where characterized by a

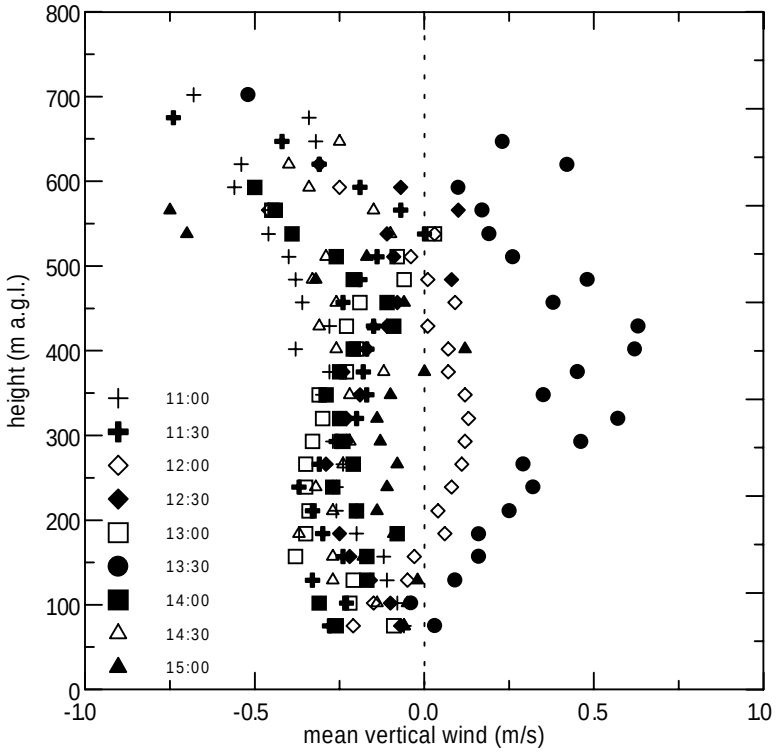

Fig. 9. – Mean vertical wind profiles for April 23, 1998, for the time periods reported in the legend.

shallow mixed layer, with relatively high values of SHF (typically about 50 Wm^{-2}) and low winds. It is likely that a cold pool of air usually dominates this layer, as can often be observed in valleys [1].

In fact, under these circumstances, the slow progressive heating of the shallow mixed layer gradually erases the overlying inversion, until it completely disappears and the first vigorous thermals begin to rise. The disappearance of the low level inversion should lead to an increase of the surface wind speed, because the very efficient mixing in the new higher PBL tends to uniform the surface wind with the wind at the higher levels. If we consider the case of April 23, 1998, such an increase of the surface wind speed is really evident (fig. 8). For the same day we can also appreciate how this event roughly occurs at the same time for which the facsimile plot of fig. 6c shows the first well-defined thermals.

As far as early morning time periods of this kind are considered, we have kept for the comparison purpose just the σ_w^3/z profiles showing at least four lined-up values, starting from heights higher than 100 m. We have also found that these circumstances always correspond to a linear correlation coefficient of about 0.99, $|\xi| > 5$ and $u < 1\ \mathrm{ms}^{-1}$ (here u indicates the mean surface wind, as measured by the anemometer). In order to reject near neutral events without undergoing a drastic reduction of valid data, we have chosen for z/L a threshold value of -0.5 instead of -1, as is common practice. The reasonability of such a choice will be however analyzed and discussed.

4·2. *Data analysis.* – As a consequence of the limitations illustrated in the previous subsection, the sub-set of cases characterized by a significant nearly linear profile has been selected for the computation of the SHF profile and to compare their mean value in the surface layer with that got from the eddy correlation method. If we consider just the central hours, *i.e.* the time periods 11:00–15:00 for winter days and 10:00–16:00 for spring days, the above-mentioned limitations lead to an overall amount of valid data of about 50%.

Typical diurnal variations for the two days for which we have performed the spectral analysis, January 16, 1998 and February 27, 1998, are illustrated in fig. 10. The upper part of this figure shows the direct comparison of the SHF extrapolated at an height of 10 m from the linear part of the σ_w^3/z profile (subsect. 3·1) and the ones calculated from anemometer's data (subsect. 3·2). The lower part of the figure shows the comparison between the PBL height trend obtained with the three different methods:

i) extrapolating the linear part of the σ_w^3/z profile up to the intersection with the height's axis;

ii) estimating on the facsimile plot the mean value, over the period under examination, of the height of the lower darker area;

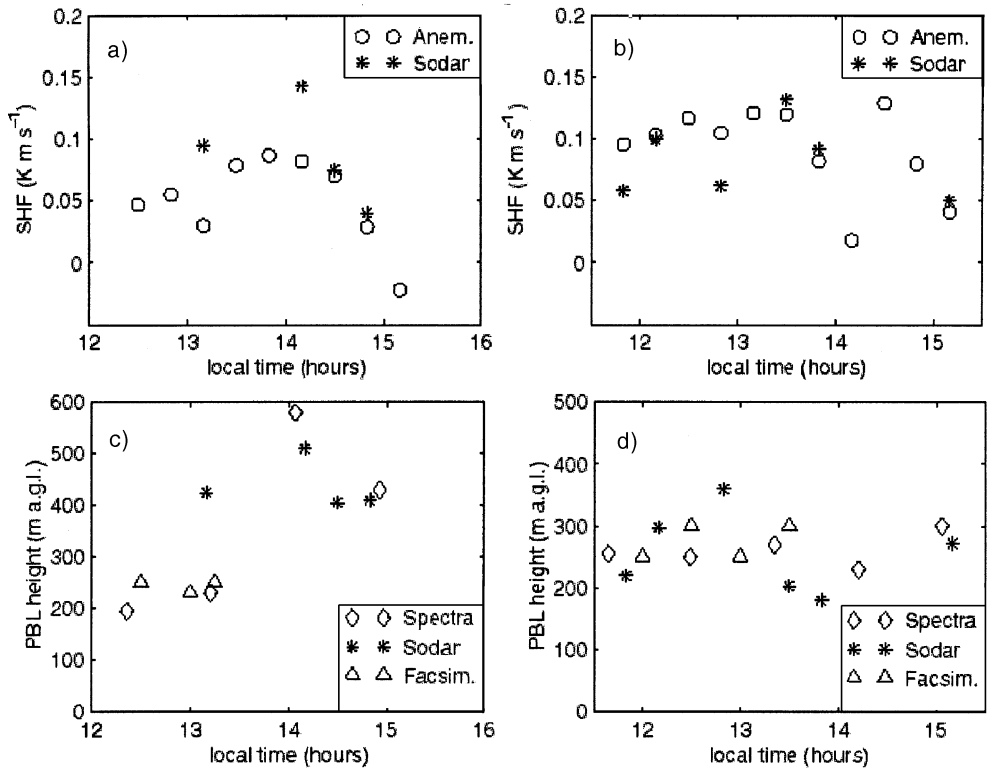

Fig. 10. – Upper part: comparison between SHF extrapolated from SODAR data and SHF calculated from anemometer's data (a) for January 16, 1998 and (b) for February 27, 1998. Lower part: comparison between the PBL height obtained with the three different methods (c) for January 16, 1998 and (d) for February 27, 1998.

iii) identifying the wavelength, $\lambda_m = \overline{U(z)}/f_m(z)$, at which the power maximum occurs and calculating z_i from (3).

The latter point needs some clarifications. In order to estimate λ_m as objectively as possible, we have performed, in the spectral sub-range nearby the maximum, a least-squares 2nd-order polynomial fit on each spectrum, considering just the spectral points corresponding to the frequencies around the maximum. As an example, for the spectra reported in fig. 3 and 4, we have chosen the interval $6 \cdot 10^{-3}\,\mathrm{Hz} < f < 1.5 \cdot 10^{-2}\,\mathrm{Hz}$. It should also be taken into account that, as far as PBL heights of the order of 200 m are considered, the mean values plotted in fig. 10c and 10d are affected by a quite large uncertainty, as explained in subsect. 3·3.

Figure 10a shows the characteristic bell-shaped diurnal variation for the SHF measured by both the SODAR and the anemometer, where the SODAR-measured SHF overestimates the SHF obtained from the anemometer. Taking into account the different averaging time of the spectral maximum retrieval and profile flux extrapolation procedure, the PBL height diurnal trend for the same day displayed in fig. 6c shows that the different methods are in good agreement.

On the contrary, the SHF and PBL height trends relative to February 27, 1998 displayed in fig. 10b and 10d, respectively, are quite particular. Moreover, from the facsimile plot relative to this day (fig. 6b), we can see that evident dome-like structures modulated by the stronger thermals are present in the higher part of the PBL. It is interesting to notice that the SHF obtained from the anemometer shows a very unusual undulating, but almost constant on average, trend between 12 and 14:30 (the sharp decrease of SHF between 13:30 an 14:00, as well as the low SHF at 13:10 of January 16, are due to the presence of a sporadic cloud).

The SODAR-measured SHF is in good agreement with the one measured by the anemometer, except than at 11:50 and 12:50, where it shows a very low value with respect to the one inferred from anemometer's data. This event is due probably to the peculiarity of the PBL evolution for this day that, at least until 14:00, presents a condition in the middle between the ones of shallow mixed layer and well-developed convection.

Also the PBL heights calculated with the different methods are in good agreement, if we exclude the SODAR-measured value at 12:50. We must also say that, in the latter case, the choice of a different linear portion of the σ_w^3/z profile, underlying the one effectively chosen, would improve greatly the agreement between SHF and PBL estimated by the SODAR and the anemometer. However, as this linear zone consisted of just three poorly lined-up σ_w^3/z values, and in order to follow a procedure as objective as possible for all cases, we have kept the values corresponding to the wider overlying linear region.

Figure 11 summarizes the results obtained for the SHF from the eight analyzed days. According to the anemometer's data analysis, we have divided the data into three classes relative to different values of the surface wind u and of z/L (obviously here z is fixed and equal to 10 m), as specified in the higher part of the legend. We also drew the correlation line $\mathrm{SHF}_{ane} = m \cdot \mathrm{SHF}_{sod} + q$ relative to all data and to each class separately, as specified in the lower part of the legend. The values of m, q and of the correlation coefficient r for the different cases are displayed in table I.

As expected, for $u < 2$ and $z/L < -1$, *i.e.* for low wind and proved convection, we have the highest r and the m closest to 1. For $u > 2$ and $z/L < -1$, *i.e.* for relatively strong wind and proved convection, we have a lower value of r and a slightly lower

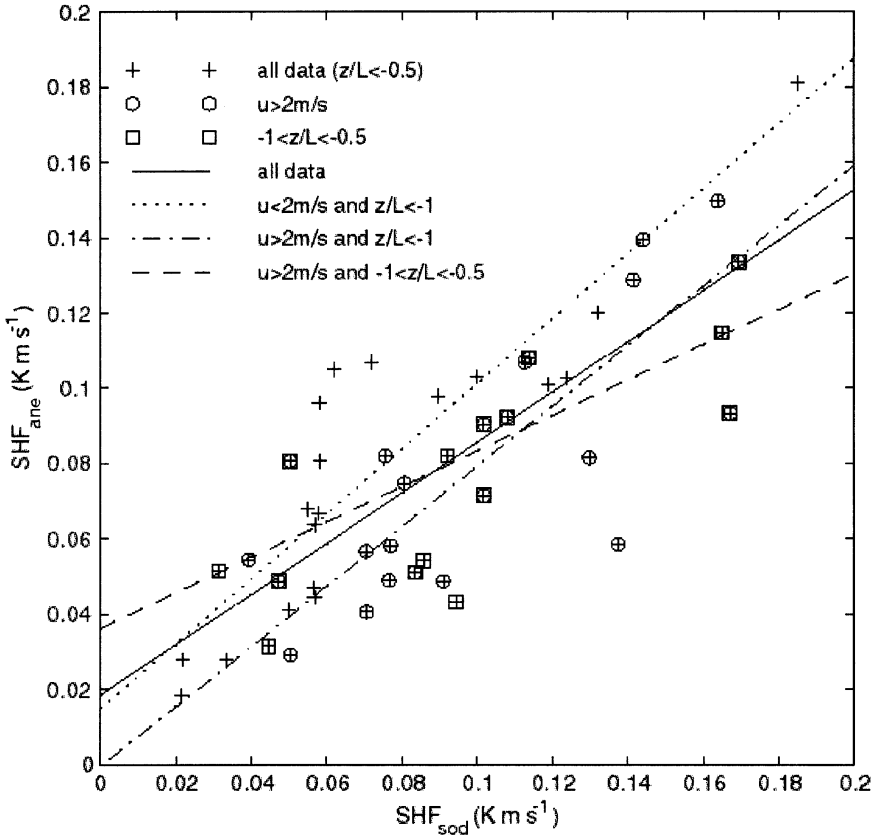

Fig. 11. – Correlation 1 to 1 for SHF calculated from SODAR and anemometer for all the days analyzed. For further explanations see the text.

value of m. This result seems reasonable, as it is an expected feature that higher wind speeds, due to the increased shear, both perturb the linearity and, on average, increase the overestimation of the SHF from the linear regression method. An interesting feature for this class is that in the lower left part of fig. 11, *i.e.* for $\mathrm{SHF}_{\mathrm{ane}} < 0.5$, the data are located under the fit line, while in the higher right part of fig. 11, *i.e.* for $\mathrm{SHF}_{\mathrm{ane}} > 0.8$, the data are located above the fit line. A behavior of this kind suggests us

TABLE I. – *Values of the angular coefficient m, the intercept q and the correlation coefficient r relative to the linear fits of* fig. 11.

Class	r	m	q (10^{-3} kms^{-1})
all data	0.79	0.67	18
$u < 2$ and $z/L < -1$	0.90	0.86	15
$u > 2$ and $z/L < -1$	0.81	0.80	− 0.50
$u > 2$ and $-1 < z/L < -0.5$	0.80	0.47	36

that a fit more complex than linear could be appropriate for such conditions, and that the equation of the regression curve should probably contain u or some related characteristic quantity.

For $u > 2$ and $-1 < z/L < -0.5$, we found a very low m, although r is almost equal to the one of the previous case. Furthermore, the data seems randomly distributed around the corresponding correlation line. We conclude that in this case, differently from the previous one, the poor estimate obtained via the least-square line is probably the best we can do.

We must also point out that the last possible case, $u < 2$ and $-1 < z/L < -0.5$, corresponding to light wind and unstable conditions approaching near neutral ones, was not analyzed due to the presence of just four points. Such a low number of points is a further indication that our starting assumption was a reasonable one. In fact, for such conditions a shear-aided convection is unlikely and so we do not expect to find a nearly linear portion of the σ_w^3/z profile in a wide number of cases. We also checked that all of these four data were relative to early morning hours.

Finally, as far as the linear fit relative to all data is concerned, we can state that it constitutes a way to obtain reliable, although almost rough, estimates of the SHF. Of course, it should be used only when just SODAR measurements are available.

5. – Conclusions

A simple parameterization of the turbulence structure in a convective PBL, based on local free convection velocity scale and mixed layer relationship, has been applied to evaluate the surface heat flux as well the PBL height just from the vertical velocity variance measured at multiple levels by a SODAR. Unlike previous works, the measurements have been performed in a region characterized by a complex terrain where the flow structure should be perturbed by the orographic forcing, and the parameterization, taking into account wind speed up to 7 m/s, has been extended to non-calm conditions. Reliable estimates of surface heat flux and PBL height are obtained in about 50% of the convective events observed, but during some periods this method could not be applied due to the absence of linearity in any portion of the σ_w^3/z profile. If we exclude the time periods characterized by a shallow mixed layer or by near neutral situations, we have found that the lack of linearity is essentially due to abrupt changes of the mean wind intensity and/or direction.

* * *

The instrumentation used in this study is provided with funds from Parco Scientifico e Tecnologico d'Abruzzo (PSTA) and Consorzio Gran Sasso. We are grateful to Dr. G. MASTRANTONIO and S. ARGENTINI of the IFA-CNR, Frascati (Roma), for the suggestions regarding the software applications and the general outlines of this work. Special thanks are due to Ing. V. VALLERIANI of PSTA, for the time she spent to furnish us the digitized map of the Aterno valley orography in a portable format and to Prof. G. VISCONTI for the supervision of the work.

REFERENCES

[1] STULL R. B., *An Introduction to Boundary Layer Meteorol.* (Kluwer Academic Publishers, Dordrecht) 1988, pp. 666.

[2] PANOFSKY H. A. and MCCORMICK R., *The Spectrum of Vertical Velocity Near Surface, Quart. J. Roy. Meteorol. Soc.*, **86** (1960) 495-503.

[3] GREENHUT G. K. and MASTRANTONIO G., *Turbulent Kinetic Energy Budget Profiles Derived from Doppler SODAR Measurements, J. Appl. Meteorol.*, **28** (1989) 99-106.

[4] WEILL A., KLAPISZ C., STRAUSS B., BAUDIN F., JAUPART C., VAN GRUNDERBEEK P. and GOUTORBE J. P., *Measuring Heat Flux and Structure Functions of Temperature Fluctuations with an Acoustic Doppler SODAR, J. Appl. Meteorol.*, **19** (1980) 199-205.

[5] FIACCONI S., PENDESINI M. I., CASSARDO C. and FRUSTACI G., *Validation of a Method for the Determination of the Sensible Heat Flux with SODAR Data in Free Convection Cases, Nuovo Cimento*, **20** (1997) 577-594.

[6] GIANNINI L., ARGENTINI S., MASTRANTONIO G. and ROSSINI L., *Estimation of Flux Parametres from SODAR Wind Profiles, Atmos. Environ.*, **31** (1997) 1307-1313.

[7] CINQUE G., BERNARDINI L., PAOLUCCI T., BIANCO L., ZAURI R., FERRETTI R. and VISCONTI G., *Local Effects of Mountains on Weather in the Central Italy: Preliminary Results from the Comparison of Wind Profiler, RASS and SODAR Data with MM5 Numerical Model*, in *Proceedings of the Symposium RADME 98, ROMA Tor-Vergata, 9-10 June 1998*.

[8] TACONET O. and WEILL A., *Convective Plumes in the Atmospheric Boundary Layer as Observed with an Acoustic Doppler SODAR, Boundary Layer Meteorol.*, **25** (1983) 143-158.

[9] KAIMAL J. C., WYNGAARD J. C., HAUGEN D. A., COTÈ O. R., IZUMI Y., CAUGHEY S. J. and READINGS C. J., *Turbulence Structure in the Convective Boundary Layer, J. Atmos. Sci.*, **33** (1976) 2152-2169.

[10] KAIMAL J. C., EVERSOLE R. A., LENSCHOW D. H., STANKOV B. B., KAHN P. H. and BUSINGER J. A., *Spectral Characteristic of the Convective Boundary Layer over Uneven Terrain, J. Atmos. Sci.*, **39** (1982) 1098-1114.

[11] KAIMAL J. C., ABSHIRE N. L., CHADWICK R. B., DECKER M. T., HOOKE W. H., KROPFLI R. A., NEFF W. D., PASQUALUCCI F. and HILDEBRAND P. H., *Estimating the Depth of the Daytime Convective Boundary Layer, J. Appl. Meteorol.*, **21** (1982) 1123-1129.

[12] MASTRANTONIO G. and FIOCCO G., *Accuracy of Wind Velocity Determinations with Doppler Sodars, J. Appl. Meteorol.*, **28** (1982) 823-830.

[13] CAUGHEY S. J. and READING C. J., *Vertical Component of Turbulence in Convective Conditions, Adv. Geophys. A*, **18** (1974) 125-130.

[14] NEFF W. D. and COULTER R. L., *Acoustic Remote Sensing*, in *Probing the Atmospheric Boundary Layer*, edited by D. H. LENSCHOW (American Meteorology Society, Boston, Mass.) 1986, pp. 201-239.

[15] SCHOTANUS P., NIEWSTADT F. T. M. and DE BRUIN H. A. R., *Temperature Measurement with a Sonic Anemometer and its Applications to Heat and Moisture Fluxes, Boundary Layer Meteorol.*, **26** (1983) 81.

[16] KAIMAL J. C. and GAYNOR J. E., *Another Look at Sonic Thermometry, Boundary Layer Meteorol.*, **56** (1991) 401-410.

[17] HIGNET P., *Correction to Temperature Measurements with a Sonic Anemometer, Boundary Layer Meteorol.*, **61** (1983) 175-187.

[18] TENNEKES H. and LUMLEY J. L., *A First Course in Turbulence* (MIT Press, Cambridge, Mass.) 1972, pp. 300.